SPE-173261-MS

A Compositional Model Fully Coupled with Geomechanics for Liquid-Rich Shale and Tight Oil Reservoir Simulation

Yi Xiong, Philip H. Winterfeld, Cong Wang, and Yu-Shu Wu, Colorado School of Mines; Zhao-Qin Huang, China University of Petroleum (East China)

This paper was prepared for presentation at the SPE Reservoir Simulation Symposium held in Houston, Texas, USA, 23–25 February 2015.

Abstract

The pore sizes of unconventional reservoir rocks, such as shale and tight rocks, are on the order of nanometers. The thermodynamic phase behavior of *in-situ* hydrocarbon mixtures in such small pores is significantly different from that of bulk fluids in the PVT cells, primarily due to effect of large capillary pressure. For example, it has been recognized that the phase envelop shifts and bubble point pressure is suppressed under subsurface condition in tight oil reservoirs. On the other hand, it has been observed that the pore sizes, especially the sizes of pore-throats, are subject to change due to rock deformation induced by the fluid depletion from over-pressurized unconventional reservoirs. As the fluids are being produced from the pore space, the effective stress on reservoir rock increases, resulting in reduction of the pore and pore-throat sizes. This reduction on pore spaces again affects the fluid flow through impacts on the thermodynamic phase behavior, as well as stress induced changes in porosity and permeability. Thus a coupled flow-geomechanics model capturing *in-situ* reservoir phase behavior is in general necessary to model tight and shale reservoir performance.

In this paper, we propose a multiphase, multidimensional compositional reservoir model, fully coupling fluid flow with geomechanics for tight and shale reservoirs. The fluid flow model is a compositional model, based on general mass conservation law for each component, incorporating both Darcy flow and molecular diffusions. The geomechanical model is derived from the thermo-poro-elasticity theory extended to multiple porous and fractured media systems; mean normal stress as the stress variable is solved simultaneously with mass conservation equations. The vapor-liquid equilibrium (VLE) calculation is performed with Peng-Robinson Equation of State (EOS) including the effects of capillary pressure on phase behaviors. The finite-volume based numerical method, integrated finite difference method, is used for space discretization for both mass conservation and stress equations. The formulations are solved fully implicitly to assure the stability.

This compositional model integrates key subsurface behaviors of unconventional shale reservoirs, such as rock compaction effect, stress-induced changes of rock properties, and stress-dependent capillary effects on VLE. We take the Eagle Ford tight oil as an example to illustrate the effects of stress-dependent capillary pressure on VLE and *in-situ* fluid properties. This model can be generally applied to both dew-point (gas condensate) and bubble-point (tight oil) systems of tight and shale reservoirs. Eventually

it could improve the forecast accuracy for long-term production rate and recovery factors of unconventional petroleum reservoirs.

Introduction

Liquid-rich shale and tight oil has been receiving great attentions recently as a type of unconventional resources, because it is more economic than shale gas as well as technologies in horizontal drilling and massive hydraulic-fracturing advance. For example, tight oil production has been very active in the past few years in U.S., increasing from less than 1 million barrels per day (MMbbl/d) in 2010 to more than 3 MMbbl/d in the second half of 2013 (EIA, 2014). Three geologic sources, Bakken, Eagle Ford, and Permian Basin formations accounts for the main productions.

Those tight formations have some similar reservoir characteristics, such as nano-pore sizes, stress-sensitive rocks, and high initial reservoir pressure etc. For example, Kuila and Prasad (2011) pointed out that shale matrix has predominantly micro-pores with less than 2 nm diameter to meso-pores with 2-50 nm diameters. Nelson (2009) claimed that the normal range for shale matrix from 5 to 50 nm. The Middle Bakken interval, pay zone of Bakken tight oil reservoir, consists of tight limestone and silt stones, with matrix pore sizes ranging from 10 nm to 50 nm (Chu et al., 2012; Nojabaei et al., 2013; Wang et al., 2013). Rafatian and Capsan (2014) used NMR (Nuclear Magnetic Resonance) logging and SEM (Scanning Electron Microscope) imaging to characterize Wolfcamp rocks, one of the most active tight oil formations in Permian Basin, and concluded two most frequent pore size distributions is about 5 nm and 80 nm.

In addition to small pore sizes, the tight reservoir formations are stress-sensitive. Stress-dependency of reservoir rock properties, especially porosity and permeability, have been attracting intensive investigations through laboratory and modeling studies in the past decades. These investigations have been extended to shale and tight rocks in the past few years, because of the attention to unconventional resources. For example, Cho et al. (2013) measured pressure-dependent natural-fracture permeability in shale and its effect on shale-gas production; Mokhtari et al. (2013) studied stress-dependent permeability anisotropy for Eagle Ford, Mancos, Green River, Bakken, and Niobrara shales. Han et al. (2013) investigated an unconventional reservoir rock with nano-Darcy permeability under true triaxial stress conditions, and claimed that stress-dependency is more pronounced in low permeability rock than in conventional reservoir rock. Besides above laboratory tests on tight rocks, Chu et al. (2012), Honarpour et al. (2012), and Orangi et al. (2011) made field observations on strong stress-dependency of tight oil reservoirs.

These characteristics of tight reservoirs differentiate them from conventional reservoirs and should be treated properly in reservoir modeling and simulations. According to Firincioglu et al. (2012), although there are other disjoining forces existing (such as van der Waals, structural and adsorption) within the small pores, capillary pressure due to significant interfacial curvature is the primary factor affecting *in-situ* thermodynamic properties of hydrocarbon mixture. The researchers have been investigating the impacts of capillary pressure on fluid properties and phase behavior since 1970s in oil and gas industry. It was found that the dew-point and bubble-point pressure were the same in the 30- to 40-US-mesh porous medium and in bulk volume (Sigmund et al., 1973), and concluded that capillary effects on vapor-liquid equilibrium (VLE) is negligible for conventional reservoirs. The recent studies on tight formation with nano-pores, however, show that the effect of capillary pressure on tight oil reservoirs cannot be ignored. Zarragoicoechea and Kuz (2004) claim that critical temperature and pressure shift for a confined fluid in a nanopore through experimental studies. In addition, it is also recognized that the bubble point pressures of tight oil reservoirs are suppressed due to pore confinement. In other words, the bubble point pressure of oil with the same composition is lower in nano-pores than measured in bulk size in PVT laboratory. Nojabaei et al. (2013) included the capillary pressure effects on fluid phase behaviors for Bakken reservoir simulation and found a better history match. Du and Chu (2012) studied the suppressed bubble point pressure with various permeability and GOR (Gas-Oil Ratio). Pang et al. (2012) analyzed impacts of pore

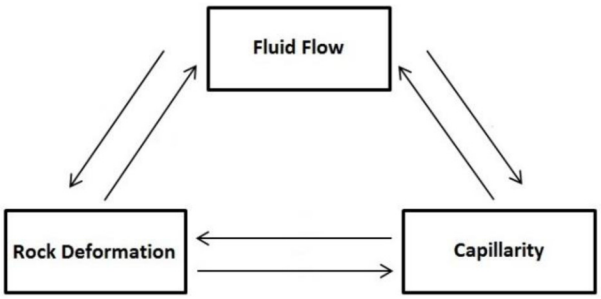

Figure 1—Conceptual diagram of the compositional model coupled with geomechanics

confinement on saturation pressures for three gas condensate systems and three oil mixtures and found non-negligible capillary effects.

On the other hand, stress-dependency rock of tight formations requires coupling between fluid flow and geomechanics. The conventional (uncoupled) reservoir simulator does not generally incorporate stress-dependent reservoir properties, and only approximates the changes of porosity as function of pore pressure through pore volume compressibility (Ahmed, 2006; Ahmed and McKinney, 2011; Aziz and Settari, 1979; Craft et al., 1991; Ertekin et al., 2001). This conventional simplification for rock deformation is not sufficient for stress-sensitive reservoir simulations. A variety of methods for coupling fluid flow and geomechanics have been proposed (Dean et al., 2006; Gutierrez et al., 2001; Minkoff et al., 2003; Settari and Walters, 2001; Tran et al., 2009). From loose to tight, there are usually three types of coupling methods, explicit coupling, iterative coupling, and fully coupling. For an explicit coupled method, the reservoir simulator performs fluid flow calculations at each time step and the flow solutions are passed to geomechanical model at selected time step for stress calculations. This approach is also called one-way coupling, because only flow solutions are passed to geomechanical model while geomechanical solutions do not feedback to flow at the same time step. With iterative coupling method, the fluid flow and geomechanics sub-systems are solved separately and sequentially at each time step. This approach is a two-way coupling, because geomechanics model exchanges solutions with fluid flow system until the total equation systems reach convergence. For a fully coupled method, the fluid flow and geomechanics variables are solved simultaneously through one set of equation system. This is most rigrous and accurate coupling method.

As discussed above, non-negligible capillary effects and flow-geomechanics coupling have been investigated and pursued separately in reservoir simulation practices. However, the integration between them is necessary for tight reservoir modeling and is not well addressed. For example, Chu et al. (2012) observes that rock compaction has a large impact on pore-throat size in Bakken formation. The pronounced change of pore-throat size leads to a significant increase of capillary pressure. Therefore the capillary pressure in tight reservoirs is not static but stress-dependent during reservoir depletion. Wang et al. (2013) related the change of capillary pressure to the change of pore pressure as table input and used it for Bakken reservoir simulations. However, it is an oversimplified method without coupling geomechanics and neglecting other stress-dependent properties. Thus the integration between non-negligible capillarity on VLE and coupled flow-geomechanics is necessary to better capture and study fluid flow behavior of tight oil reservoirs.

In this paper, we propose a compositional model fully coupled with geomechanics with the capability to perform VLE calculations under stress-dependent capillary pressure. Figure 1 presents the conceptual model, consisting of fluid flow, rock deformation and capillarity, and their interlays among them. Fluid flow affects the stress state through change of pore pressure due to reservoir production; rock deformation feed backs to flow through induced changes of reservoir properties. High capillary pressure in tight

reservoirs has non-negligible effects on VLE and accordingly affects fluid properties. In addition, the capillary pressure is not static but stress-dependent therefore interrelates to rock deformation.

The remaining of the paper discusses the mathematical models for fluid flow, geomechanics, and VLE calculations. The finite volume based method, integrated finite difference (IFD), is used for space discretization; and the resulting discretized nonlinear equations are solved fully implicitly to assure stability. The flow and stress equations are solved simultaneously with Newton/Raphson method. The rock properties, such as porosity and permeability, are updated according to current stress at each Newtonian iteration. The VLE calculations are based on Peng-Robinson EOS (Peng and Robinson, 1976) with capillarity effect. Finally we will take Eagle Ford oil to demonstrate the effects of stress-dependent capillary pressure on *in-situ* fluid properties.

Mathematical Model

A general compositional model is derived from the law of mass balance and Equation (1) is the governing mass balance equation for each mass component.

$$F_i + q_i = \frac{\partial N_i}{\partial t} \tag{1}$$

where subscript i is the index for mass component, $i = 1,\ldots,n_c, n_w$ with n_c being the total number of hydrocarbon components and n_w being the water component. We assume that there is no mass transfer between the hydrocarbon (oil and gas) and water phases. F is the mass flux term; q is the sink/source term per unit volume of reservoir; the right hand side N is mass accumulation term, denoting the moles per unit volume of reservoir. Accumulation term N_i can be evaluated as follows by relating to phase molar density p, saturation S, and component mole fraction in oil and gas phases x_i and y_i,

$$N_i = \phi(\rho_o S_o x_i + \rho_g S_g y_i) \tag{2}$$

where $i = 1,\ldots,n_c$ donating hydrocarbon components. For water the accumulation term is evaluated as below.

$$N_w = \phi\rho_w S_w \tag{3}$$

The mass flux term F for hydrocarbon component and water are evaluated below.

$$F_i = -\nabla\cdot\left(\rho_o x_i \mathbf{v}_o + \rho_g y_i \mathbf{v}_g\right) + \nabla\cdot\left(D_{g,i}\nabla\left(\rho_g y_i\right)\right) \tag{4}$$

$$F_w = -\nabla\cdot\left(\rho_w \mathbf{v}_w\right) \tag{5}$$

For hydrocarbon component, mass flux is evaluated with Darcy's law in both oil and gas phases, and molecular diffusion in gas phase only. v_β is Darcy velocity of phase β, defined by Darcy's law for multiphase fluid flow.

$$\mathbf{v}_\beta = -\frac{kk_{r\beta}}{\mu_\beta}(\nabla P_\beta - \rho_\beta g\nabla Z) \tag{6}$$

The coupled geomechanical model is based on the classical theory of poro-thermal-elastic system (Jaeger et al., 2007; Zoback, 2007), and obeys a generalized version of Hooke's law:

$$\sigma_{ij} - (\delta\alpha P + 3\beta K\Delta T) = 2G\varepsilon_{ij} + \lambda\delta_{ij}\varepsilon_v \tag{7}$$

where σ is stress and subscripts i, j represent the directions; it is normal stress if $i = j$, otherwise shear stress; δ_{ij} is Kronecker delta, given by $\delta_{ij} = 1$ if $i = j$ otherwise $\delta_{ij} = 0$.α is Biot's coefficient; P is reservoir pore pressure; ΔT is the temperature difference from the reference temperature at a thermally unstrained state; β is linear thermal expansion coefficient; K, G and λ are mechanical properties of rock, representing

bulk modulus, shear modulus, and Lame's constant, respectively. ε stands for strain; and ε_v is volumetric strain evaluated as $\varepsilon_v = \varepsilon_{xx} + \varepsilon_{yy} + \varepsilon_{zz}$. Two other fundamental relations in the linear elasticity theory are the relationship between strain tensor and displacement vector and the condition of static equilibrium as Equation (8) and (9).

$$\varepsilon_{ij} = \frac{1}{2}\left(\frac{\delta u_i}{\delta x_j} + \frac{\delta u_j}{\delta x_i}\right) \tag{8}$$

$$\nabla \cdot \bar{\bar{\sigma}} + \overline{F_b} = 0 \tag{9}$$

where u is the displacement and F_b is the body force. Combine Equations (7), (8) and (9) to obtain the thermo-poro-elastic Navier Equation:

$$\nabla(\alpha P + 3\beta KT) + (\lambda + G)\nabla(\nabla \cdot \bar{u}) + G\nabla^2 \bar{u} + \bar{F}_b = 0 \tag{10}$$

Take divergence of Equation (10) to yield the equation with only one term containing the displacement vector:

$$\nabla^2(\alpha P + 3\beta KT) + (\lambda + 2G)\nabla^2(\nabla \cdot \bar{u}) + \nabla \cdot \bar{F}_b = 0 \tag{11}$$

The divergence of displacement vector $\nabla.\bar{u}$ is the volumetric strain ε_v:

$$\nabla \cdot \bar{u} = \frac{\partial u_x}{\partial x} + \frac{\partial u_y}{\partial y} + \frac{\partial u_z}{\partial z} = \varepsilon_{xx} + \varepsilon_{yy} + \varepsilon_{zz} = \varepsilon_v \tag{12}$$

On the other hand, the trace of the stress tensor is an invariant with the same value for any coordinate system. Thus Equation (7) gives the trace of Hooke's law for a thermo-poro-elastic medium as follows.

$$\sigma_m - (\alpha P + 3\beta K \Delta T) = (\lambda + \frac{2}{3}G)\varepsilon_v = K\varepsilon_v \tag{13}$$

Finally combining Equations (11), (12) and (13) yields the governing geomechanical equation relating mean stress, pore pressure, temperature and body force as Equation (14). The coefficient of each term is functions of Poisson's ratio only.

$$\nabla \cdot \left[\frac{3(1-\nu)}{1+\nu}\nabla\sigma_m + \bar{F}_b - \frac{2(1-2\nu)}{1+\nu}\nabla(\alpha P + 3\beta KT)\right] = 0 \tag{14}$$

Phase Equilibrium Calculations

A two phase (oil and gas) equilibrium calculation method is required to perform phase separation and calculate fluid properties of each phase. In a multi-component system under vapor-liquid equilibrium, the chemical potential μ of each component i throughout all co-existing phases should be equal. This general requirement becomes a practical engineering tool if the chemical potential can be related to measurable or calculable quantities (Danesh, 1998), such as fugacity f as follows.

$$\mu_i^o = \mu_i^g \quad or \quad f_i^o = f_i^g \quad i = 1,...,n_c \tag{15}$$

The practical way to calculate fugacity of each component is to evaluate the dimensionless fugacity coefficient Φ, which is defined as the ratio of fugacity to partial pressure of the corresponding phase for component i:

$$\Phi_i^o = \frac{f_i^o}{x_i P^o} \qquad \Phi_i^g = \frac{f_i^g}{y_i P^g} \qquad i = 1,...,n_c \tag{16}$$

Equilibrium ratio of component i defined as $K_i = y_i / x_i$ is related to fugacity coefficient in a non-ideal system by combining Equation (15) and (16),

$$K_i = \frac{y_i}{x_i} = \frac{P^o \Phi_i^o}{P^g \Phi_i^g} = \frac{P^o \Phi_i^o}{(P^o + P_{cgo})\Phi_i^g} \tag{17}$$

In conventional reservoirs, Equation (17) is simplified to $K_i = \Phi_i^{\,0} / \Phi_i^{\,g}$ by assuming $P^0 \approx P^g$; however this assumption is not valid for tight oil reservoirs due to small pore size or large capillary pressure P_{cgo}.

Rachford-Rice (R-R) equation (Rachford Jr and Rice, 1952) takes equilibrium ratio as input for flash calculation as Equation (18) to solve compositions of oil and gas phases.

$$\sum_{i=1}^{n_c} \frac{z_i(K_i - 1)}{\tilde{n}_o + K_i(1 - \tilde{n}_o)} = 0 \tag{18}$$

One practical way to obtain equilibrium ratio is to calculate fugacity coefficient, which can be related rigorously to measurable properties using thermodynamic relations (Danesh, 1998) as below.

$$ln\Phi_i = \frac{1}{RT}\int_V^\infty [(\frac{\partial P}{\partial N_i})_{T,V,N_{j\neq i}} - RT/V]dV - \ln Z \tag{19}$$

Equation (19) can be determined with the aid of the Peng-Robinson Equation of State (EOS), relating pressure, temperature, volume and compositions.

The overall phase equilibrium calculation requires iterative computation because Equation (19) can only be computed after flash calculation with Equation (18), which in turn needs the K_i as input. Therefore an initial guess of K_i is required as the starting point. In this paper, Wilson's correlation (Wilson, 1969) is used to generate the initial guesses for equilibrium ratios.

Constitutive Relations

The mass conservation equations, geomechanical equation, and two phase equilibrium calculations need to be supplemented with constitutive equations, which relate all the parameters as functions of a set of primary variables of interest.

Saturation and Volume Constraints

Saturation constraint as Equation (20) relates the saturations of three phases; volume constraint as Equation (21) associates phase moles per reservoir volume and phase molar density to porosity; that is the sum of phase volumes per unit reservoir volume equals porosity. In addition, the saturations correspond to phase volume fraction and can be obtained in terms of moles and molar density of phases as Equation (22).

$$S_w + S_o + S_g = 1 \tag{20}$$

$$N_w/\rho_w + N_o/\rho_o + N_g/\rho_g = \phi \tag{21}$$

$$S_\beta = \frac{N_\beta/\rho_\beta}{\sum_\beta N_\beta/\rho_\beta} \qquad \beta = o, g, w \tag{22}$$

Compositional Constrains

The following compositional constrains hold in general.

$$\sum_{i=1}^{n_c} x_i = 1 \qquad \sum_{i=1}^{n_c} y_i = 1 \qquad \sum_{i=1}^{n_c} z_i = 1 \qquad \tilde{n}_o + \tilde{n}_g = 1 \tag{23}$$

$$\sum_{i=1}^{n_c} N_i = N_o + N_g \tag{24}$$

$$z_i = \tilde{n}_o x_i + \tilde{n}_g y_i \tag{25}$$

Capillary Pressure Functions

The capillary pressures are needed to relate pressures between phases, and they also play important roles on *in-situ* thermodynamic properties for tight reservoirs. The water and gas phase pressures are related by capillary pressure between them, P_{cqw}, which is function of water saturation only.

$$P_w = P_g - P_{cgw}(S_w) \tag{26}$$

The oil phase pressure is related to gas phase pressure by assuming capillary pressure between them is a function of two saturations of water and oil phases respectively.

$$P_o = P_g - P_{cgo}(S_w, S_o) \tag{27}$$

In a water wet system, the oil-water capillary pressure P_{cwo} in a three-phase system is defined as below.

$$P_{cow} = P_{cgw} - P_{cgo} = P_o - P_w \tag{28}$$

Relative Permeability Functions

The relative permeability is functions of phase saturation in three-phase system described below.

$$k_{rw} = k_{rw}(S_w) \qquad k_{rg} = k_{rg}(S_g) \qquad k_{ro} = k_{ro}(S_w, S_g) \tag{29}$$

Effects of Geomechanics on Reservoir Properties

The coupled geomechanics feeds back to fluid flow through its effects on reservoir properties, which in turn affect mass accumulation and two-phase equilibrium described below.

Effective Stress

Terzaghi (1936) initially defined the effective stress as the difference between normal stress and pore pressure, and Biot (1957) generalize it as:

$$\sigma' = \sigma_m - \alpha P \tag{30}$$

where σ' is effective stress and α is Biot or effective stress coefficient.

Porosity and Permeability

Reservoir porosity and absolute permeability are functions of effective stress, especially for stress-sensitive tight reservoirs. It is also assumed that rock deformation has no or negligible effects on relative permeability.

$$\phi = \phi(\sigma') \qquad k = k(\sigma') \tag{31}$$

Mass Accumulation under Rock Deformation

The volume of a grid block is subject to change due to rock deformation, which is incorporated into simulation model by volumetric strain, ε_v, solved at Newtonian iteration step. The following equation describes the way to evaluate mass accumulation under rock deformation effect.

$$N_i = (1-\varepsilon_v)\phi\left(\rho_o S_o x_i + \rho_g S_g y_i\right) \tag{32}$$

where $i = 1, \ldots, n_c$ donating hydrocarbon components and for water:

$$N_w = (1-\varepsilon_v)\phi\rho_w S_w \tag{33}$$

Capillary Pressure

As discussed above, capillary pressure is critical to model tight reservoirs because of its non-negligible effect on vapor-liquid equilibrium. It could be evaluated with well-known Young-Laplace equation as

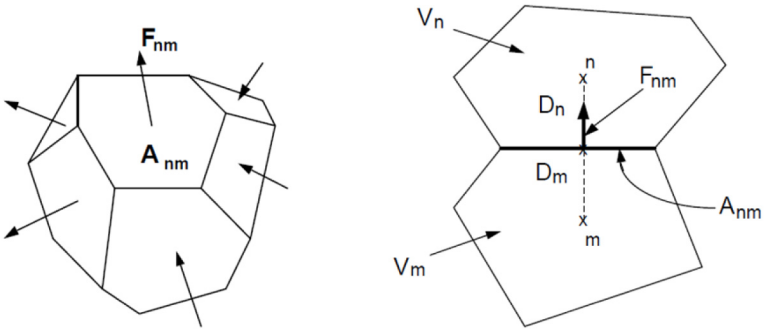

Figure 2—Space discretization and geometry data in the integral finite difference method (Pruess, 1991)

Equation (34), where the interfacial tension (IFT) value is usually estimated with composition data and Parachor values (Weinaug and Katz, 1943) as Equation (35).

$$P_c = \frac{2IFT\cos\theta}{r} \tag{34}$$

$$\sigma^{\frac{1}{4}} = \sum_{i=1}^{N_c} P_{\sigma i}\left(x_i\rho_o - y_i\rho_g\right) \tag{35}$$

Nojabaei (2013) and Wang (2013) pointed out that Young-Laplace equation may give underestimated capillary pressure value, much less than the actual measurement, because of very low IFT calculated with Equation (35) for tight oil system. Thus we apply Leverett J-function (Leverett, 1941) to scale the stress-dependent capillary pressure, relative on a reference value. We also add one coefficient to account for the difference of fluid composition between current and reference states.

$$P_c = CP_{c0}\sqrt{\frac{k_0\phi}{k\phi_0}} \tag{36}$$

where P_{c_o} is non-deformed capillary pressure at reference state; k_0 and k are reference permeability and current stress-induced permeability respectively; similarly for ϕ_0 and ϕ; C is a function of current fluid composition.

Numerical Model

Numerical Discretization

The integral finite-difference (IFD) method (Narasimhan and Witherspoon, 1976; Pruess, 1991) is used for space discretization. Figure 2 presents the space discretization and geometry data in IFD method; the left figure shows a grid block or arbitrary REV (representative elementary volume) V_n, and it has flux F_{nm} at surface A_{nm}; the right figure shows the geometry of two neighboring grid blocks.

With the IFD method, make volumetric integration on Equation (1) over REV, V_n, to get:

$$\int_{V_n} -\nabla\cdot(\rho_o x_i\vec{v}_o + \rho_g y_i\vec{v}_g)dV + \int_{V_n}\nabla\cdot\left(D_{g,i}\nabla\left(\rho_g y_i\right)\right)dV + \int_{V_n} q_i dV = \int_{V_n}\frac{\partial\phi(\rho_o S_o x_i + \rho_g S_g y_i)dV}{\partial t} \tag{37}$$

Apply divergence theorem to Equation (37) to convert volume integral to surface integral for flux term; replace volume integrals with volume average; and surface integral is evaluated with discrete sum of fluxes over surface average segments; the discretized equation is obtained and written in residual form as Equation (38), where η_n is the set of neighboring grid blocks directly connecting grid blocks n; λ is the phase mobility defined as $\lambda_\beta = k_{r\beta}/\mu_\beta$ for phase β; ψ is the flow potential, including both pressure and gravity term; subscript $nm + 1/2$ denotes a proper averaging at the interface between n and m; $t + 1$ is the current time step and t is the previous time step. γ is the transmissivity defined as Equation (39). The water component has similar form of discretized equation written in Equation (40),

$$R_{i,n}^{t+1}=\frac{\left[V\phi(\rho_o S_o x_i+\rho_g S_g y_i)\right]_n^{t+1}-\left[V\phi(\rho_o S_o x_i+\rho_g S_g y_i)\right]_n^{t}}{\Delta t}-\sum_{m\in\eta_n} D_{g,i}A_{nm}^{t+1}\frac{(\rho_g y_i)_m^{t+1}-(\rho_g y_i)_n^{t+1}}{d_n^{t+1}+d_m^{t+1}}$$
$$-\sum_{m\in\eta_n}[(\rho_o x_i\lambda_o)_{nm+\frac{1}{2}}^{t+1}\gamma_{nm}^{t+1}(\Psi_{om}^{t+1}-\Psi_{on}^{t+1})+(\rho_g y_i\lambda_g)_{nm+\frac{1}{2}}^{t+1}\gamma_{nm}^{t+1}(\Psi_{gm}^{t+1}-\Psi_{gn}^{t+1})]-(Vq_i)_n^{t+1}=0 \tag{38}$$

$$\gamma_{nm}^{t+1}=\left(\frac{A_{nm}k_{nm+\frac{1}{2}}}{d_n+d_m}\right)^{t+1} \tag{39}$$

$$R_{w,n}^{t+1}=\frac{\left(V\phi\rho_w S_w\right)_n^{t+1}-\left(V\phi\rho_w S_w\right)_n^{t}}{\Delta t}-\sum_{m\in\eta_n}\left[(\rho_w\lambda_w)_{nm+\frac{1}{2}}^{t+1}\gamma_{nm}^{t+1}(\Psi_{wm}^{t+1}-\Psi_{wn}^{t+1})\right]-(Vq_w)_n^{t+1}=0 \tag{40}$$

Note that, different from the conventional fully implicit method, the volume V and porosity ϕ of grid block n, flow transmissivity γ_{nm} and other geometry data are evaluated at each time step and iteration level due to rock deformation effects.

The geomechanical governing equation can also be discretized with IFD method. Take volume integral on Equation (14) and apply divergence theorem on it to get the following surface integral form (Winterfeld and Wu, 2014; Xiong et al. 2013):

$$\int_{\Gamma_n}[\frac{3(1-\nu)}{1+\nu}\nabla\sigma_m+\bar{F}_b-\frac{2(1-2\nu)}{1+\nu}\nabla(\alpha P+3\beta KT)]\cdot\hat{n}d\Gamma_n=0 \tag{41}$$

The surface integral is evaluated with discrete sum over surface average segments at current time step, and the discretized geomechanical governing equation can be written in residual form below.

$$R_{\sigma,n}^{t+1}=\sum_{m\in\eta_n}\left[\frac{3(1-\nu)}{1+\nu}\frac{\sigma_n^{t+1}-\sigma_m^{t+1}}{d_{nm}}+(\bar{F}_b\cdot\hat{n})_{nm}-\frac{2(1-2\nu)}{1+\nu}\left(\alpha\frac{P_n^{t+1}-P_m^{t+1}}{d_{nm}}+3\beta K\frac{T_n-T_m}{d_{nm}}\right)\right]A_{nm}=0 \tag{42}$$

Numerical Solution Method

According to Gibbs phase rule, the thermodynamic degrees of freedom for a compositional system are $n_m + 2 - n_p$, which fix the intensive state of the system; there are also $n_p - 1$ saturation degrees of freedom. Thus the final degrees of freedom for an isothermal compositional system $f = (n_m + 2 - n_p) + (n_p - 1) - 1 = n_m$ where n_m is the number of total mass component and n_p is the number of phases in the system. The compositional model in this paper is fully coupled with geomechanics having mean stress as another degree of freedom. Thus the total degrees of freedom is $n_m + 1$ or $n_c + 2$, because n_m includes n_c hydrocarbon components and one water component in the system.

The number of independent primary variables should equal to the total degrees of freedom of the system $n_c + 2$, which corresponds to $n_c + 2$ residual non-linear equations, Equations (38), (40), and (42), for each grid block V_n. We choose pressure of oil phase P_0, hydrocarbon mole fractions Z_1,. . ., Z_{nc-1}, water saturation S_w, and mean stress σ_m as the $n_c + 2$ primary variables. Thus for a system with n_b grid blocks there are $n_b \times (n_c + 2)$ equations and primary variables. For a non-linear equation $R_{\kappa,n}^{t+1}$ of grid block V_n, where $\kappa = 1, \ldots, n_c + 2$, the Newton/Raphson scheme give rise to

$$R_{\kappa,n}^{t+1}\left(\boldsymbol{x}_{p+1}^{t+1}\right)=R_{\kappa,n}^{t+1}\left(\boldsymbol{x}_{p}^{t+1}\right)+\sum_k\frac{\partial R_{\kappa,n}^{t+1}\left(\boldsymbol{x}_{p}^{t+1}\right)}{\partial x_k}\left(x_{k,p+1}-x_{k,p}\right)=0 \tag{43}$$

where index $k = 1,. . ., n_2 + 2$ represents primary variable $1,. . .,n_c+2$ respectively; p is the iteration level for current time step $t + 1$; $n = 1,. . ., n_b$ donates the index for grid blocks. Equation (43) can be written as

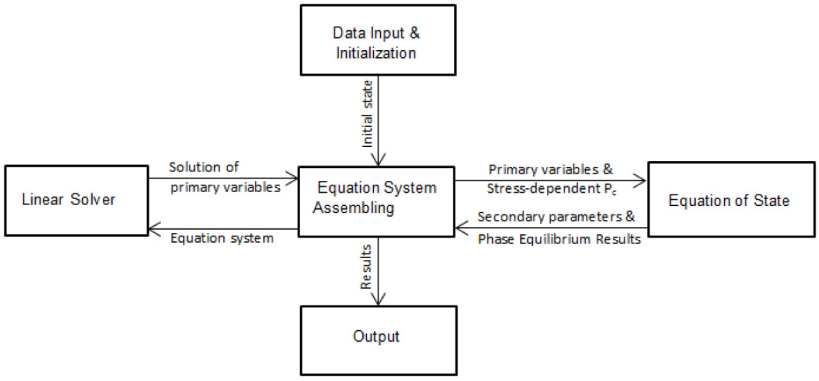

Figure 3—Program structure and core modules

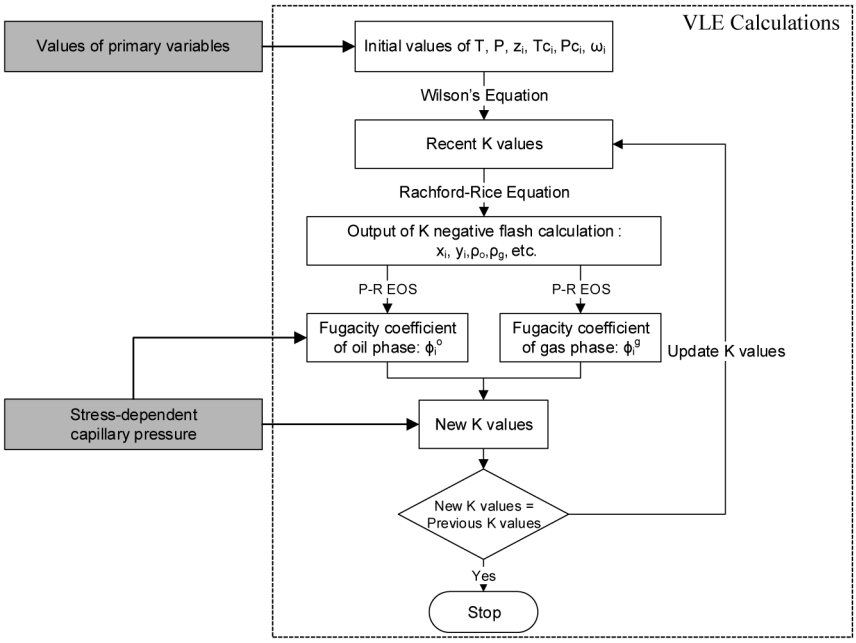

Figure 4—Procedure of Peng-Robinson EOS based vapor-liquid equilibrium calculation (EOS module)

$$\sum_k \frac{\partial R_{\kappa,n}^{t+1}\left(\boldsymbol{x}_p^{t+1}\right)}{\partial x_k}\left(x_{k,p+1}-x_{k,p}\right)=-R_{\kappa,n}^{t+1}\left(\boldsymbol{x}_p^{t+1}\right) \tag{44}$$

Equation (44) represents a set of $n_b \times (n_c + 2)$ linear equations for increments $(x_{k,\,p+1} - x_{k,\,p})$. All terms $\partial R_{\kappa,n}^{t+1}\left(\boldsymbol{x}_p^{t+1}\right)/\partial x_k$ in the Jacobian matrix are evaluated by numerical differentiation.

Program Structure and Procedures

Collins et al. (1992) pointed out that phase equilibrium calculation is by itself a difficult task and it adds a high level of complexity to final solutions for solving flow and equilibrium simultaneously. In this paper we treat phase equilibrium calculation in an encapsulated EOS module from flow calculation as shown in Figure 3.

Figure 3 also shows the data exchanged between modules. For example, the EOS module receives the primary variables and stress-dependent capillary pressure to perform VLE calculation, and generate secondary parameters, such as phase density, viscosity and saturation etc. Figure 4 presents the detailed procedures of EOS module for vapor-liquid equilibrium calculations. The right dashed-line box is the EOS module itself, and it is associated with primary variables and capillary pressures.

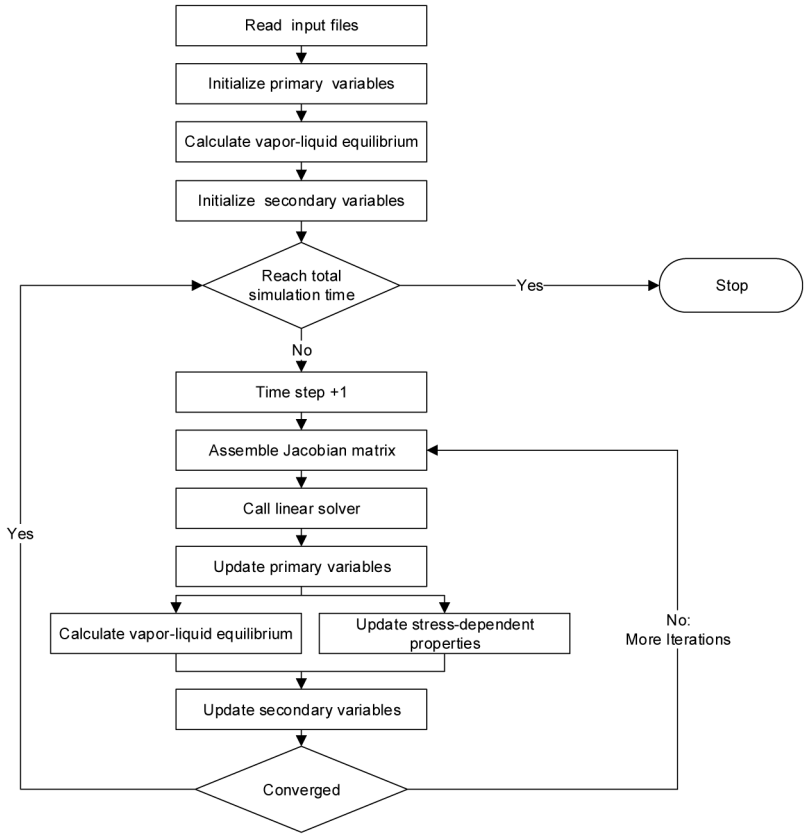

Figure 5—Overall simulation procedures

Figure 5 shows the overall simulation procedures. It follows a general simulation process and includes coupled geomechanics. The initialization part reads the input files and initializes primary variables. The secondary variables are initialized through VLE calculations with initial primary variables as input. The time looping starts after initialization and continues until reach total simulation time. Each Newtonian iteration includes assembling Jacobian matrix, solving linear equation system, updating primary variables with solutions, calculating the secondary variables with updated solutions. The iteration continues until reaching convergence where simulation updates stress-dependent reservoir properties and moves to next time step.

Case Studies

In this section we take Eagle Ford tight oil composition from published data to demonstrate the effects of stress-dependent capillary pressure on in-situ fluid properties. Tables 1 and 2 shows the oil composition, EOS parameters and Peng-Robinson interaction coefficients used in the calculations.

In this demonstration we use Young-Laplace Equation to estimate capillary pressure of Eagle Ford oil because the measured data of capillary pressure of Eagle Ford formation is not available. With Equation (35), above composition data gives interfacial tension ranging from 3 to 10 mN/m in two phase region. Nojabaei (2013) and Wang (2013) state that Young-Laplace equation may give underestimated capillary pressure value than actual measured data for tight oil reservoirs; thus we use the upper range 10 mN/m in this demonstration. Rylander et al. (2013) measured pore and pore throat distribution of Eagle Ford shale and conclude that median pore throat diameter is estimated to range from 10 nm to 35 nm. Chu et al. (2012) claimed that the reduction of pore-throat size is within 20% to 60% due to rock deformation for tight oil reservoirs. With above published data and correlations, the estimated data of stress-dependent capillary pressure for Eagle Ford formation is generated shown in Table 3.

Table 1—Eagle Ford composition data and EOS parameters (Orangi et al., 2011)

Component	Molar Fraction	Pc (psi)	Tc (°R)	Vc (ft^3/lbm)	Acentric Factor	Molar Weight
C1	0.31231	673.1	343.3	1.5658	0.013	16.04
N2	0.00073	492.3	227.2	1.4256	0.04	28.01
C2	0.04314	708.4	549.8	2.3556	0.0986	30.07
C3	0.04148	617.4	665.8	3.2294	0.1524	44.1
CO2	0.01282	1071.3	547.6	1.5126	0.225	44.01
IC4	0.0135	529.1	734.6	4.2127	0.1848	58.12
NC4	0.03382	550.7	765.4	4.1072	0.201	58.12
IC5	0.01805	483.5	828.7	4.9015	0.2223	72.15
NC5	0.02141	489.5	845.6	5.0232	0.2539	72.15
NC6	0.04623	439.7	914.2	5.9782	0.3007	86.18
C7+	0.16297	402.8	1065.5	7.4093	0.3739	114.4
C11+	0.12004	307.7	1223.6	10.682	0.526	166.6
C15+	0.10044	241.4	1368.4	14.739	0.6979	230.1
C20+	0.07306	151.1	1614.2	26.745	1.0456	409.2

Table 2—Peng-Robinson Interaction Coefficients (Orangi et al., 2011)

	C1	N2	C2	C3	CO2	IC4	NC4	IC5	NC5	NC6	C7+	C11+	C15+	C20+
C1	0	0.036	0	0	0.1	0	0	0	0	0	0.025	0.049	0.068	0.094
N2	0.036	0	0.05	0.08	-0.02	0.095	0.09	0.095	0.1	0.1	0.151	0.197	0.235	0.288
C2	0	0.05	0	0	0.13	0	0	0	0	0	0.02	0.039	0.054	0.075
C3	0	0.08	0	0	0.135	0	0	0	0	0	0.015	0.029	0.041	0.056
CO2	0.1	-0.02	0.13	0.135	0	0.13	0.13	0.125	0.125	0.125	0.11	0.097	0.085	0.07
IC4	0	0.095	0	0	0.13	0	0	0	0	0	0.01	0.019	0.027	0.038
NC4	0	0.09	0	0	0.13	0	0	0	0	0	0.01	0.019	0.027	0.038
IC5	0	0.095	0	0	0.125	0	0	0	0	0	0.005	0.01	0.014	0.019
NC5	0	0.1	0	0	0.125	0	0	0	0	0	0.005	0.01	0.014	0.019
NC6	0	0.1	0	0	0.125	0	0	0	0	0	0	0	0	0
C7+	0.025	0.151	0.02	0.015	0.11	0.01	0.01	0.005	0.005	0	0	0	0	0
C11+	0.049	0.197	0.039	0.029	0.097	0.019	0.019	0.01	0.01	0	0	0	0	0
C15+	0.068	0.235	0.054	0.041	0.085	0.027	0.027	0.014	0.014	0	0	0	0	0
C20+	0.094	0.288	0.075	0.056	0.07	0.038	0.038	0.019	0.019	0	0	0	0	0

Table 3—Estimated stress-dependent capillary pressure of Eagle Ford formation

Change of Effective Stress (psi)	Pore Throat Size Multiplier	Pore Throat Size (nm)	Capillary Pressure (psi)
0	1.00	30.0	48.3
1000	0.84	25.2	57.6
2000	0.60	18.0	80.6
3000	0.53	15.9	91.2
4000	0.48	14.4	100.7
5000	0.45	13.5	107.4
6000	0.42	12.6	115.1
7000	0.40	12.0	120.9

Figure 6 presents the comparison of bubble point pressures between neglected effect of capillary pressure and the effect of stress-dependent capillary pressure data of Table 3 with reservoir temperature 237 °F. It is observed that the bubble point pressure is suppressed due to capillary pressure effect on VLE; rock deformation increases the effective stress and exaggerates the suppression due to decrease of pore throat size and increase of capillary pressure. The bubble point pressure reduces from 2,030 psi to about

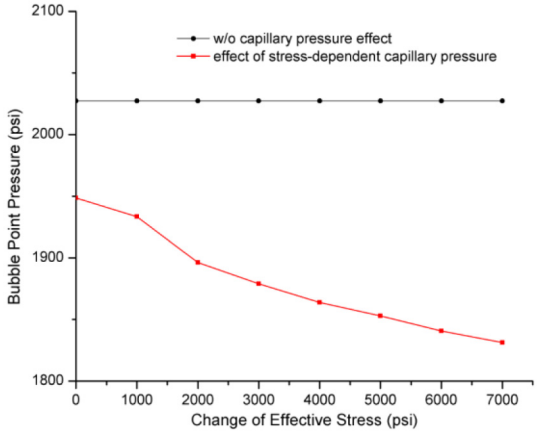

Figure 6—Effect of stress-dependent capillary pressure on bubble point pressure

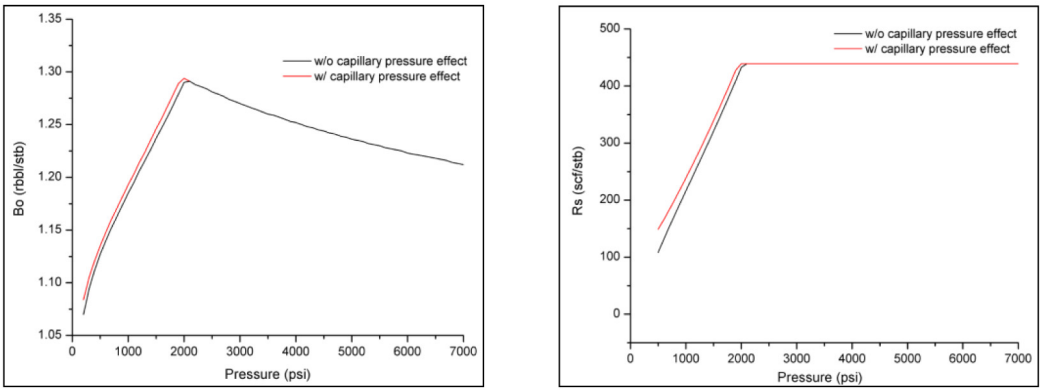

Figure 7—Effect of capillary pressure on oil formation volume factor and gas solubility

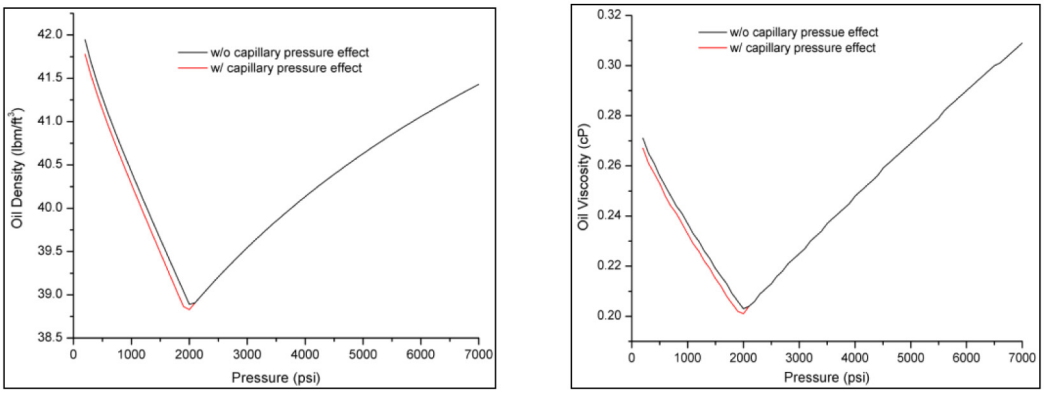

Figure 8—Effect of capillary pressure on oil density and viscosity

1,950 psi with the effect of 48.3 psi capillary pressure on VLE. The increase of effective stress further suppresses bubble point pressure to 1,830 psi.

Figure 7 shows the effect of capillary pressure on oil formation volume factor B_o and gas solubility R_s. The capillary pressure not only suppresses bubble point pressure, but also leads to higher values of B_o and R_s in two phase region because less light components evolve from oil to gas phase. The increase of effective stress results in higher capillary pressure thus could further shift B_o and R_s curves.

The effect of capillary pressure on oil density and viscosity is shown in Figure 8. The calculation of oil viscosity from compositions is based on Lorentz-Bray-Clark (LBC) correlation (Lohrenz et al., 1964).

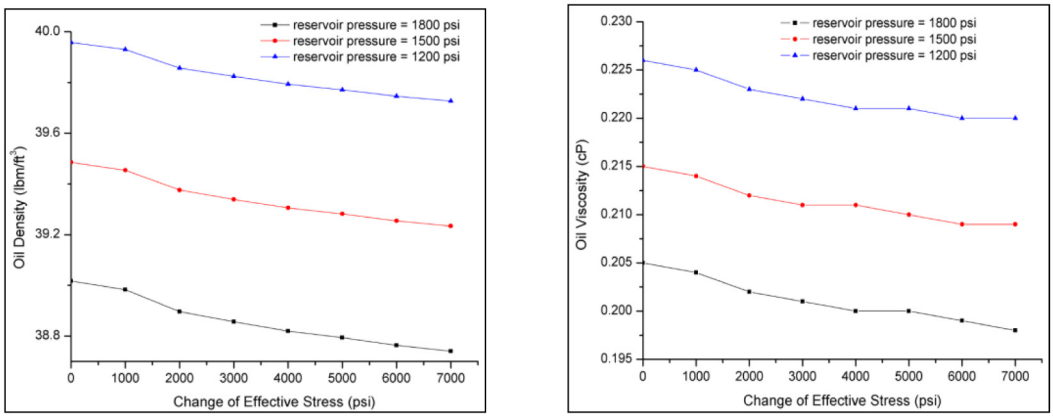

Figure 9—Oil density and viscosity change as the change of effective stress

Oil density and viscosity are lower at the same reservoir pressure under the effect of capillary pressure in two phase region, because the bubble point suppression results in more light components remaining in oil phase. The oil density and viscosity are also functions of the change of effective stress due to stress-dependent capillary pressure. The increase of effective stress exaggerates the suppression of bubble point pressure, which keeps more light components in oil phase and further reduces oil density and viscosity shown in Figure 9, which presents the reduction of oil density and viscosity as increase of effective stress at different reservoir pressures.

Above results are based on the estimated data in Table 3 and the capillary pressures are calculated with Young-Laplace equation, which may underestimate capillary pressures of tight oil system. Thus the real effects of stress-dependent capillary pressure on reservoir phase behaviors and fluid properties could be more pronounced. Although the example we presented is a tight oil system, the VLE calculations with capillary effect can be extended to shale gas and gas condensate reservoirs (Wang and Wu, 2014).

Conclusions

In this paper we formulate a compositional model fully coupled with geomechanics for liquid-rich shale and tight oil reservoir simulations. The compositional model is based on a general multi-phase multi-component framework with mass conservation law of each component as governing equations. The vapor-liquid equilibrium (VLE) calculation is encapsulated from flow equation system with the advantage that a variety of approaches of VLE calculations could be used without affecting flow equations. The pore confining effect is treated through incorporating capillary pressure into the VLE calculation with Peng-Robinson Equation of State. The coupled geomechanical model is derived from classical theory of poro-thermal-elastic system with mean stress as another variable instead of total stress tensor. This coupling approach has the advantages of less computation workload and easier fully coupled with flow equations. Although the mean stress model cannot analyze shear stress induced phenomena, it is rigorous in handling rock deformation effects in flow-focused reservoir simulations.

We take Eagle Ford tight oil as an example to illustrate the effects of stress-dependent capillary pressure on VLE and fluid properties. The bubble point pressure is suppressed and the suppression is exaggerated due to induced reduction of pore throat size by rock deformation. The fluid properties, such as oil density, viscosity, oil formation volume factor, and gas solubility, are different in a two phase region from those without capillarity effect on VLE. This difference is explained by more light components remaining in oil phase because of suppressed bubble point pressure. The postponed gas phase appearance as well as lower oil density and viscosity favor the liquid production from tight oil reservoirs. Rock deformation further complicates fluid flow behaviors because it affects both VLE through reduced pore-throat size and reservoir rock properties. The compositional model we presented has the capability

to capture the complex flow behaviors of tight oil reservoirs. Although the example we presented is a bubble-point system, this compositional model can be generally extended to dew-point (gas condensate) system of tight and shale reservoirs. Eventually it could improve the forecast accuracy for long-term production rate and recovery factors of unconventional reservoirs.

Acknowledgement

The authors would like to extend thanks to Energy Modeling Group (EMG) of Petroleum Engineering Department at Colorado School of Mines and Foundation CMG for the support and sponsor of this research.

Nomenclature

A	Interface area between grid blocks [ft^2]
D	Coefficient of molecular diffusion [ft^2/day]
F_b	Body force [lbf]
F	Mass flux per unit volume of reservoir [lbmol/ft^3/day]
f	Fugacity of component in oil or gas phase [psi]
G	Shear modulus [psi]
K	Equilibrium ratio of component [-]
k	Absolute permeability [md]
k_r	Relative permeability of phases [-]
N	Mass accumulation per unit volume of reservoir [lbmol/ft^3]
n_c	Total number of hydrocarbon components [-]
n_b	Total number of grid blocks [-]
$\tilde{n}$	Mole fraction of oil or gas phase over whole hydrocarbon system [-]
P	Reservoir pressure [psi]
P_c	Capillary pressure [psi]
P_σ	Parachor value [-]
q	Sink/source per unit volume of reservoir [lbmol/ft^3/day]
R	Ideal gas constant [ft^3psiR^{-1}lbmol^{-1}]
S	Saturation of water, oil or gas phase [-]
T	Temperature [°F]
t	Time [days]
u	Displacement [ft]
V	Volume [ft^3]
$\vec{v}$	Darcy velocity of water, oil or gas phase [ft/day]
x	Molar fraction in oil phase [-]
y	Molar fraction in gas phase [-]
Z	Compressibility factor [-]
z	Total molar fraction in hydrocarbon system of component [-]
α	Biot coefficient [-]
β	Linear thermal expansion coefficient [R^{-1}]
Φ	Fugacity coefficient [-]
ϕ	Reservoir porosity [-]
σ	Stress [psi]
ρ	Molar density of water, oil or gas phase [lbmol/ft^3]
μ	Viscosity [cP]
μ	Chemical potential [psi]

ε_v	Volumetric strain [-]
λ	Lames constant [psi]
ν	Poisson's ratio [-]
ψ	Flow potential [psi]
η	A set of neighboring grid blocks of a grid block [-]

Subscripts

g	Gas phase
i	Index of mass component
k	Index of primary variables
m	Mean stress
n	Index of grid block
$nm+1/2$	A proper averaging at the interface between grid blocks n and m
o	Oil phase
p	Iteration level
w	Water phase
β	Fluid phase
κ	Index of primary equations
0	Reference state

Superscripts

t	Time step level

References

Ahmed, T. (2006), *Reservoir engineering handbook,* third edn, Gulf Professional Publishing.

Ahmed, T. and McKinney, P. (2011), *Advanced reservoir engineering,* Gulf Professional Publishing.

Aziz, K. and Settari, A. (1979), *Petroleum reservoir simulation,* Vol. **476,** Applied Science Publishers London.

Biot, M. A. (1957), 'The elastic coefficients of the theory of consolidation', *J. appl. Mech.* **24,** 594–601.

Cho, Y., Ozkan, E., Apaydin, O. G. et alet al. (2013), 'Pressure-dependent natural-fracture permeability in shale and its effect on shale-gas well production', *SPE Reservoir Evaluation & Engineering* **16**(02), 216–228.

Chu, L., Ye, P., Harmawan, I. S., Du, L. and Shepard, L. R. (2012), 'Characterizing and simulating the nonstationariness and nonlinearity in unconventional oil reservoirs: Bakken application', in SPE Canadian Unconventional Resources Conference, 30 October-1 November, Calgary, Canada.

Collins, D., Nghiem, L., Li, Y.-K. and Grabenstetter, J. (1992), 'An efficient approach to adaptive-implicit compositional simulation with an equation of state', *SPE reservoir engineering* **7**(2), 259–264.

Craft, B., Hawkins, M. and Terry, R. (1991), *Applied petroleum reservoir engineering,* Old Tappan, NJ (USA); Prentice Hall Inc.

Danesh, A. (1998), *PVT and phase behaviour of petroleum reservoir fluids,* Vol. **47,** Elsevier.

Dean, R. H., Gai, X., Stone, C. M. and Minkoff, S. E. (2006), 'A comparison of techniques for coupling porous flow and geomechanics', *SPE Journal* **11**(1), 132.

Du, L. and Chu, L. (2012), 'Understanding anomalous phase behavior in unconventional oil reservoirs', in SPE Canadian Unconventional Resources Conference, 30 October-1 November, Calgary, Canada.

EIA, U. (2014), '*Annual energy outlook 2014*', US Energy Information Administration, Washington, DC.

Ertekin, T., Abou-Kassem, J. H. and King, G. R. (2001), *Basic applied reservoir simulation,* Richardson, TX: Society of Petroleum Engineers.

Firincioglu, T., Ozkan, E. and Ozgen, C. (2012), 'Thermodynamics of multiphase flow in unconventional liquids-rich reservoirs', in SPE Annual Technical Conference and Exhibition, October 8-10, San Antonio, TX.

Gutierrez, M., Lewis, R. and Masters, I. (2001), 'Petroleum reservoir simulation coupling fluid flow and geomechanics', *SPE Reservoir Evaluation & Engineering* **4**(03), 164–172.

Han, G., Gutierrez, M. and Schmitz, P. (2013), 'Stress-dependent flow mechanical and acoustic properties for an unconventional oil reservoir rock', in Unconventional Resources Technology Conference, 12-14 August, Denver, CO.

Jaeger, J. C., Cook, N. G. and Zimmerman, R. (2007), *Fundamentals of rock mechanics,* fourth edn, John Wiley & Sons.

Kuila, U. and Prasad, M. (2011), 'Understanding pore-structure and permeability in shales', in SPE Annual Technical Conference and Exhibition, 30 October-2 November, Denver, CO.

Leverett, M. (1941), 'Capillary behavior in porous solids', *Transactions of the AIME* **142**(01), 152–169.

Lohrenz, J., Bray, B. G., Clark, C. R. et alet al. (1964), 'Calculating viscosities of reservoir fluids from their compositions', *Journal of Petroleum Technology* **16**(10), 1171–1176.

Minkoff, S. E., Stone, C. M., Bryant, S., Peszynska, M. and Wheeler, M. F. (2003), 'Coupled fluid flow and geomechanical deformation modeling', *Journal of Petroleum Science and Engineering* **38**(1), 37–56.

Mokhtari, M., Alqahtani, A. A., Tutuncu, A. N. and Yin, X. (2013), 'Stress-dependent permeability anisotropy and wettability of shale resources', in Unconventional Resources Technology Conference, 12-14 August, Denver, CO.

Narasimhan, T. and Witherspoon, P. (1976), 'An integrated finite difference method for analyzing fluid flow in porous media', *Water Resources Research* **12**(1), 57–64.

Nelson, P. H. (2009), 'Pore-throat sizes in sandstones, tight sandstones, and shales', *AAPG bulletin* **93**(3), 329–340.

Nojabaei, B., Johns, R. T. and Chu, L. (2013), 'Effect of capillary pressure on phase behavior in tight rocks and shales', *SPE Reservoir Evaluation & Engineering* **16**(03), 281–289.

Orangi, A., Nagarajan, N. R., Honarpour, M. M. and Rosenzweig, J. J. (2011), 'Unconventional shale oil and gas-condensate reservoir production impact of rock fluid and hydraulic fractures', in SPE Hydraulic Fracturing Technology Conference, 24-26 January, The Woodlands, TX.

Pang, J., Zuo, J. Y., Zhang, D. and Du, L. (2012), 'Impact of porous media on saturation pressures of gas and oil in tight reservoirs', in SPE Canadian Unconventional Resources Conference, 30 October-1 November, Calgary, Canada.

Peng, D.-Y. and Robinson, D. B. (1976), 'A new two-constant equation of state', *Industrial & Engineering Chemistry Fundamentals* **15**(1), 59–64.

Pruess, K. (1991), '*TOUGH2: A general-purpose numerical simulator for multiphase fluid and heat flow*', Technical report, Lawrence Berkeley Lab., CA (United States).

Rachford, Jr, H. and Rice, J. (1952), 'Procedure for use of electronic digital computers in calculating flash vaporization hydrocarbon equilibrium', *Journal of Petroleum Technology* **4**(10), 19–3.

Rafatian, N. and Capsan, J. (2014), 'Petrophysical characterization of the pore space in permian wolfcamp rocks', in SPWLA 55th Annual Logging Symposium, 8-22 May, Abu Dhabi, United Arab Emirates.

Rylander, E., Singer, P., Jiang, T., Lewis, R., McLin, R. and Sinclair, S. (2013), '*NMR T2 distributions*

in the eagle ford shale: Reflections on pore size', 10-12 April, The Woodlands, TX.

Settari, A. and Walters, D. A. (2001), 'Advances in coupled geomechanical and reservoir modeling with applications to reservoir compaction', *SPE Journal* **6**(03), 334–342.

Sigmund, P., Dranchuk, P., Morrow, N. and Purvis, R. (1973), 'Retrograde condensation in porous media', *Society of Petroleum Engineers Journal* **13**(02), 93–104.

Terzaghi, v. K. (1936), 'The shearing resistance of saturated soils and the angle between the planes of shear', in Proceedings of the 1st International Conference on Soil Mechanics and Foundation Engineering, Vol. **1,** pp. 54–56.

Tran, D., Nghiem, L. and Buchanan, L. (2009), 'Aspects of coupling between petroleum reservoir flow and geomechanics', in 43rd US Rock Mechanics Symposium & 4th US-Canada Rock Mechanics Symposium, American Rock Mechanics Association.

Wang, C. and Wu, Y. S. (2014), 'Modeling Analysis of Transient Pressure and Flow Behavior at Horizontal Wells with Multi-Stage Hydraulic Fractures in Shale Gas Reservoirs', in SPE Unconventional Resources Conference, 1-3 April, The Woodlands, Texas.

Wang, Y., Yan, B. and Killough, J. (2013), 'Compositional modeling of tight oil using dynamic nanopore properties', in SPE Annual Technical Conference and Exhibition, Society of Petroleum Engineers.

Weinaug, C. F. and Katz, D. L. (1943), 'Surface tensions of methane-propane mixtures', *Industrial & Engineering Chemistry* **35**(2), 239–246.

Wilson, G. M. (1969), 'A modified redlich-kwong equation of state, application to general physical data calculations', in 65th National AIChE Meeting, Cleveland, OH.

Winterfeld, P. H. and Wu, Y.S. (2014), 'Simulation of CO2 sequestration in brine aquifers with geomechanical coupling', in *Computational Models for CO2 Geo-sequestration & Compressed Air Energy Storage,* CRC Press, 275–303.

Xiong, Y., Fakcharoenphol, P., Winterfeld, P. H., Zhang R. and Wu Y.S. (2013) 'Coupled geomechanical and reactive geochemical model for fluid and heat flow: application for enhanced geothermal reservoir', in SPE Reservoir Characterization and Simulation Conference and Exhibition, 16-18 September, Abu Dhabi, UAE.

Zarragoicoechea, G. J. and Kuz, V. A. (2004), 'Critical shift of a confined fluid in a nanopore', *Fluid phase equilibria* **220**(1), 7–9.

Zoback, M. D. (2007), *Reservoir geomechanics,* Cambridge University Press.